

On how the optical depth tunes the effects of ISM on debris disks

F. Marzari¹ and P. Thebault²

¹*Dept. of Physics, University of Padova, 35131 Italy*

²*Observatoire de Paris, Meudon, Paris, France*

Accepted; Received; in original form

ABSTRACT

The flux of ISM neutral atoms surrounding stars and their environment affects the motion of dust particles in debris disks, causing a significant dynamical evolution. Large values of eccentricity and inclination can be excited and strong correlations settle in among the orbital angles. This dynamical behaviour, in particular for bound dust grains, can potentially cause significant asymmetries in dusty disks around solar type stars which might be detected by observations. However, the amount of orbital changes due to this non-gravitational perturbation is strongly limited by the collisional lifetime of dust particles. We show that for large values of the disk’s optical depth the influence of ISM flow on the disk shape is almost negligible because the grains are collisionally destroyed before they can accumulate enough orbital changes due to the ISM perturbations. On the other hand, for values smaller than 10^{-3} , peculiar asymmetric patterns appear in the density profile of the disk when we consider 1-10 μm grains, just above the blow-out threshold. The extent and relevance of these asymmetries grow for lower values of the optical depth. An additional sink mechanism, which may prevent the formation of large clumps and warping in the disks is related to the fast inward migration due to the drag component of the forces. When a significant eccentricity is pumped up by the ISM perturbations, the drag forces (Poynting-Robertson and in particular ISM drag) drive the disk particles on fast migrating tracks leading them into the star on a short timescale. It is then expected that disks with small optical depth expand inside the parent body ring all the way towards the star while disks with large optical depth would not significantly extend inside.

Key words: Celestial Mechanics – ISM: atoms – acceleration of particles

1 INTRODUCTION

The observable part of debris disks are small ($\leq 1\text{ mm}$) dusty or icy grains, collisionally produced from larger, undetectable parent bodies. In addition to the gravitational pull of the star, these grains are also affected by several forces such as stellar radiation pressure, Poynting-Robertson (PR) drag and the possible gravitational influence of large bodies in the neighborhood. As has been shown in numerous numerical studies, the combined effect of these different forces can lead to complex spatial structures in resolved disks (e.g. Wyatt 2008). A less investigated additional force that could have an influence on grain dynamics is the drag due to particles from the surrounding interstellar medium (ISM). The effect of ISM has first been addressed by Artymowicz & Clampin (1997), who studied the level of disk erosion due to sandblasting by ISM dust grains. They concluded that, at least around massive stars, this effect was negligible because small ISM grains felt a strong repulsive

radiation force. More recently, Scherer (2000), Debes et al. (2009), Maness et al. (2009), Belyaev & Rafikov (2010) and Pastor (2011) considered instead the effect of ISM *neutral atoms* on disk grains. This flux of neutral atoms acts indeed similarly to the solar wind or radiation pressure from a physical point of view but, being monodirectional, can significantly perturb the trajectories of the grains, and potentially induce asymmetric structures in the disk. In particular Maness et al. (2009) and Debes et al. (2009) suggest that the ISM flux can explain the unusual morphology of some debris disks like HD61005 and HD32997. In their model Debes et al. (2009) consider dust particles close to the blow-out size for the star and compute the trajectories of perturbed grains over a timescale of 5000 yrs. The majority of their grains are strongly perturbed and end up quickly on hyperbolic orbits. A similar scenario is outlined by Maness et al. (2009) where they concentrate on small grains ($0.1\ \mu\text{m}$) whose lifetime before ejection is of the order of a few 10^3 years. The morphology changes they observe is

mostly due to the fast transfer of grains from low eccentricity orbits into hyperbolic trajectories.

In this paper we take these studies a step further and we concentrate on the effects of the ISM neutral flow on bound Keplerian orbits of dust particles in debris disks around solar type stars. The orbital changes on relatively large dust grains (we model grains with radius ranging from 1 to 10 μm) is slow and it occurs on timescales of the order of 10^6 yrs. This timescale is much longer than that considered in Debes et al. (2009) and Maness et al. (2009) and it is related to the larger size of the grains. In addition, our grains are bound to the star and the orbital evolution induced by the ISM flow lead to eccentric and possibly asymmetric disks, characterized by density clumps, only if the collisional lifetime of the grains allows it. Thus, a crucial parameter that controls the efficiency of the ISM flow in shaping debris disks is their geometrical optical depth, on which collisional lifetimes directly depend. The collisional cascade that is steadily eroding, by cratering and fragmentation, all solid bodies in a debris disk, does indeed reduce the lifetime of dust grains, thus limiting the amount of time their trajectories can be perturbed by non-gravitational forces like radiation pressure, PR drag and interaction with ISM (Wyatt 2005). To correctly evaluate the impact of ISM on the density profile of a dust disk we thus need to account for the limited lifetime of individual particles and the amount of orbital changes that they can accumulate during that time.

The role of collisions had been discarded by Debes et al. (2009) and Maness et al. (2009) because their dust grains are pushed on hyperbolic trajectories by the ISM flow on a very short timescale (a few 10^3 years), comparable to the collisional lifetime of the particles they handle. In our scenario, grains remain on bound orbits but a simple numerical integration of dust trajectories over a long timespan, performed to predict the overall disk density distribution, can lead to misleading result which are correct only for disks with very low optical depth. A numerical model intended to evaluate the impact of ISM on the morphology of dense disks must include an estimate of the lifetime of each individual particle that will be part of the disk only for an interval of time no longer than its collisional lifetime after which it will be replaced by a new one. If the integration time of the whole particle ensemble is a few times longer than the lifetime of the considered dust particles, we will obtain a stationary relaxed population of grains which will describe in a reliable way the spatial distribution of the debris disk. We must also account that dust of different sizes would have different lifetimes so the presence of density structures would depend on the size of the dust that is imaged.

The effect of ISM neutral atom flux on the dust grain trajectories is twofold. On one side it forces a coupled evolution of eccentricity and pericenter longitude that drives the particles on aligned eccentric orbits. On the other side, if the ISM flow is inclined with respect to the parent body orbital plane a significant inclination can be pumped up. In addition, a fast inward migration is forced by the PR drag, which is strong for highly eccentric orbit, and by the ISM drag component of the force related to difference between the monodirectional velocity of the ISM neutral atoms and the orbital velocity of the dust particles. When they migrate close to the star, the grains either sublimate or impact potential planets or the star itself going lost. This is an addi-

tional sink mechanism, purely dynamical, which contributes to the erosion of the dust population.

In this paper we intend to address these issues concentrating on the balancing between the orbital evolution of dust grains in dusty disks under the effect of ISM neutral atoms perturbations and collisional lifetime. Our goal is to outline the features of the steady state population of dust produced by the combination of these effects. We will explore the amount of asymmetry in the debris disk created by the ISM perturbations and how this depends on the optical depth of the disk. We concentrate in particular on dust grains of 1 μm size since these particles, which are just above the cut-off size imposed by radiation pressure ($\sim 0.6 \mu\text{m}$), are those that dominate the geometrical cross section of the system, and thus the flux coming from the disk in the visible and near-IR (see for example Thebault & Augereau (2007)). We will also give a hint to the evolution of 10 μm size particles to test how the density distribution of the disks depends on the observed particle size.

2 THE NUMERICAL MODEL

Our numerical integration scheme computes the trajectories of a large number of dust particles of a given size using RADAU (Everhart 1985). It is a very precise algorithm that accurately handles highly eccentric orbits as those produced by ISM perturbations. It is an implicit Runge-Kutta integrator of 15th-order which proceeds by sequences within which the substeps are taken at Gauss-Radau spacings. High orders of accuracy are obtained with relatively few function evaluations. In addition, after the first sequence, the information from previous sequences is used to improve the accuracy and the integrator itself chooses the next sequence size depending on the estimated variability of the 'force' term in the differential equations. Non-gravitational forces like radiation pressure and PR drag are included as in Marzari & Vanzani (1994) and, in addition, we model the effects of the ISM neutral gas atoms adopting the same approach used to calculate the solar wind pressure (Scherer (2000)). The acceleration of a dust particle due to the impact with fast neutral atoms of the ISM wind is computed as:

$$\mathbf{f} = -C_D(n_H m_H)A_s |\mathbf{v} - \mathbf{v}_H| (\mathbf{v} - \mathbf{v}_H) \quad (1)$$

where v is the orbital velocity of the dust grain and v_H is the velocity of the ISM neutral atoms. m_H and n_H are the mass and density of neutral hydrogen atoms, respectively, $A_s = \pi r^2$ is the area of the dust particle of radius r while C_D is a drag coefficient whose value is about 2.5. This functional dependence is robust only in the limit where the gas of the ISM has a temperature lower than about 5000 K. Under this condition, the thermal speed is lower than v_H and the momentum change is proportional to the $(v - v_H)^2$. For hot ($T > 5000\text{K}$) ISM clouds the momentum change would be proportional to $(v - v_H)$ (Belyaev & Rafikov 2010; Draine & Salpeter 1979).

For the collisional lifetime of each particle, we adopt the usual expression

$$t_c \sim \frac{T}{12\tau} \quad (2)$$

where τ is the local geometrical vertical optical depth of the disk and T the orbital period of massless particles at this location (e.g. Artymowicz & Clampin 1997). Although detailed numerical studies (e.g., Thebault & Augereau (2007)) show that real collision rates may strongly depart from this simplified expression, we adopt it here for its simplicity and because it is an easy way to tune in the collisional effects.

Particle size is a crucial parameter since it determines the response to radiation pressure parameterized by β , the ratio of radiation pressure to stellar gravity. Given the steep size distribution for collisional cascades and the limited number of test particles in a deterministic code, it is impossible to consider a wide size range. We thus restrict our study to several independent simulations each with single size particles. These different runs can then be combined, when properly weighted, to give a first-order estimate of "real" disks. We consider a scenario where the central body is a solar type star and the dust grains of the debris disk are the by-product of collisions occurring in a ring of parent bodies (planetesimals, asteroids, comets) on circular orbits. Whenever a dust particle is produced, its orbital elements are computed from the position and velocity vectors of the parent body accounting for the reduced gravity $1 - \beta$ due to radiation pressure. The average collisional lifetime t_c is derived for the particle and, at starting, a random value of 'age' t_a is given to each grain. As the integration advances, t_a is updated with the timestep Δt . When t_a becomes larger than the collisional lifetime t_c , the particle is eliminated from the sample and a new one is generated with new orbital elements and $t_a = 0$. When the timespan of the integration is a few times longer than t_c we have a steady state population of dust particles where the collisional lifetime determines for how long a grain is subject to non-gravitational perturbations. In addition, when a particle is injected on a hyperbolic orbit or it has migrated far inside the parent body ring it is discarded and a new one is generated. As a consequence, the steady state population can be due to a balance between the different mechanisms of dust elimination i.e. collisions, ejection out of the system or inwards migration. We assume in our model that the parent bodies are large enough not to be significantly affected by ISM. This is a reasonable assumption since the forces acting on the particles strongly depend on their size. Larger parent bodies would be affected by ISM only on a much longer timescale.

3 INITIAL SETUP

We consider as a test case for our modeling a disk produced by a ring of parent bodies evenly distributed in between 50-70 AU on circular orbits. Since the size of the ring is small, assuming a uniform distribution is a good approximation. We adopt different values for the optical depth of the disk ranging from $\tau \sim 10^{-3}$, typical of dense collision-dominated disks like that around Beta Pictoris, to $\tau \sim 10^{-6}$ for almost collisionless disks similar to the Kuiper Belt where transport mechanisms like PR drag, stellar or ISM winds can dominate. The ISM gas flow is approximated as a monodirectional flux moving along the x-axis with a velocity of 20 km/s and a concentration of neutral hydrogen atoms equal to $n_H = 0.1 \text{ cm}^{-3}$. These are typical values of the interstellar cloud surrounding our solar system. The local speed

of the sun with respect to the ISM is around $25 \pm 2 \text{ km/s}$ but some deceleration of the interstellar neutral hydrogen flow across the heliospheric interface is expected reducing the speed to about 22 km/s (Lallement 2005). The density we adopt in the numerical model is intermediate between the value given by Fahr (1996) equal to $n_H = 0.05 \text{ cm}^{-3}$ and that given in Frisch et al (1999) of $n_H = 0.22 \text{ cm}^{-3}$.

4 THE COPLANAR CASE: (E, ϖ) EVOLUTION

We first assume that the interstellar gas flow lies on the plane of the parent body ring. This may be considered a test bench where to study the evolution of the (e, ϖ) orbital elements. In effect, it may not be a realistic scenario since the flow, impinging on one side of the disk, may not reach with equally intensity the other side being eventually absorbed. This does not occur when there is some inclination between the dust orbits and the ISM flow. However, it is useful to explore the density distribution in the planar case since the structures and clumpings that develop in the $(x - y)$ plane are retrieved when a low inclination between the flux and the initial dust orbits is assumed. In Fig.1 the position of $1 \mu\text{m}$ size particles are given after an evolution lasting about 3 times the average collisional lifetime for the case with $\tau = 1 \times 10^{-3}$ ($\Delta t = 0.5 \text{ Myr}$) and $\tau = 1 \times 10^{-4}$ ($\Delta t = 5 \text{ Myr}$, about twice T_{stark} defined by formula (7)). In the case with $\tau = 1 \times 10^{-6}$ the collisional timespan is around 100 Myr, however the fast inward evolution due to the large eccentricity, achieved by the dust grains because of the ISM perturbations, significantly limits the lifetime of the particle within the disk. The most relevant sink mechanism in this scenario is related to the fast inward migration of grains driven by both the PR drag and the ISM drag components of the force.

The density plots are derived by computing the number of particles populating the local spatial area (equal size squared bins) at the end of the numerical simulation. This number is then normalized to the total number of particles which is kept constant and equal to 4×10^4 in all our simulations.

The first plot on the top left in Fig.1 shows how the debris disk appears when the ISM force is neglected. It is axis-symmetric with a density peak at the internal ring corresponding to the location of the parent bodies. This is where all the pericenters of the particles reside and the higher density is due both to the geometrical configuration (the orbit is tangent to the circle) and to the creation of new grains when the older ones are destroyed. A second peak in the density plot appears at the outer ring where the apocenters of the particles are located and the grains move at the lowest speed. The pericenter longitudes are randomly distributed in between 0 and 360° when the steady state is reached. The initial eccentricities of our sample of particles are encompassed between 0.42-0.45 while the initial semimajor axes range from 90 to 120 AU. This orbital distribution is due to the value of β adopted at the beginning of the simulation that reduces the mass of the central star injecting the grains into eccentric orbits.

When the ISM effects are included, asymmetries develop in the disk due to the eccentricity and pericenter evolution forced by the ISM perturbation. These asymmetries

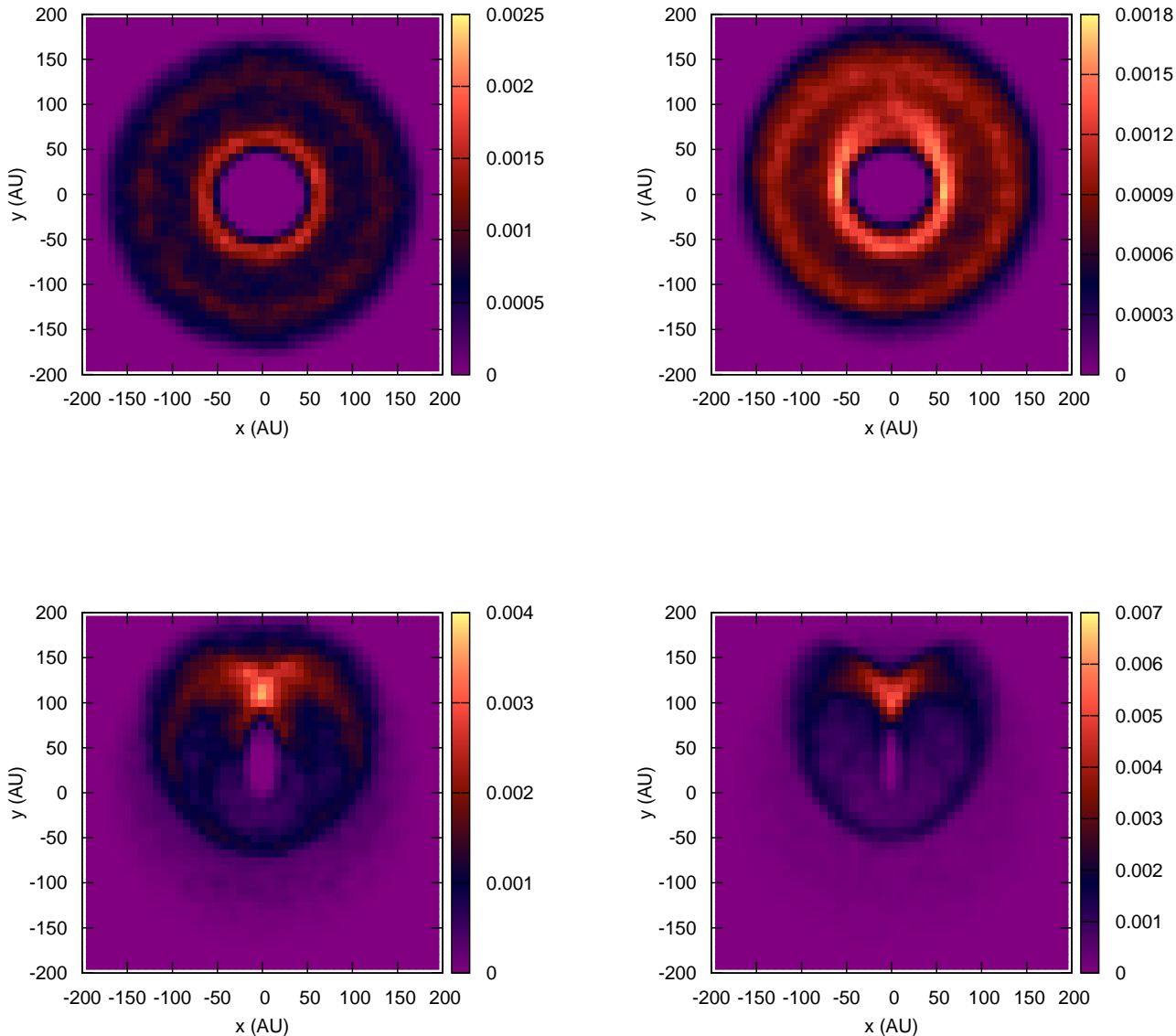


Figure 1. 2-D density distribution of $1 \mu\text{m}$ size dust particles in debris disks generated by a ring of parent bodies moving on circular orbits in between 50–70 AU. The density is computed as number of particles populating a squared region at a given timestep divided by the total number of particles in the model. The top-left plot shows how the disk appears when the ISM flow on the grains is neglected. The top-right plot illustrates the density distribution when ISM is acting on the particles and the optical depth is $\tau = 1 \times 10^{-3}$. The two bottom plots show the density distribution when $\tau = 1 \times 10^{-4}$ and $\tau = 1 \times 10^{-6}$, respectively.

are barely detectable when $\tau = 10^{-3}$ (Fig.1, upper right plot) but they become more pronounced for lower values of τ (Fig.1, bottom plots) since the grains have more time to accumulate the perturbative effects. When $\tau = 10^{-3}$ the two peaks at the particles pericenters and apocenters are still visible but the disk begins to develop an eccentric shape. The alteration in the disk shape is more noteworthy for $\tau = 10^{-6}$ when the disk appears as the superposition of two ellipses.

This feature can be explained by inspecting the orbital

behaviour of the grains under the effect of the ISM neutral gas. In Fig.2 we show the evolution with time of the grain orbits in the (e, ϖ) plane. Particles evolve towards high eccentricity values (~ 1) while, at the same time, the pericenter values tend to 270° . When large values of eccentricity are achieved, the particles drift quickly inside because of the drag component of the forces.

This behaviour can be interpreted on the basis of the analytical solution of the classical Stark problem

(Belyaev & Rafikov 2010; Pastor 2011) where the Keplerian motion of the particle is perturbed by an external force constant in magnitude and direction. In effect, the dust particle dynamics is different from that predicted by the classical Stark problem since it includes PR drag which is a tangential force. In addition, the ISM force depends on the difference between the particle v and the neutral atom velocity v_H so that the force changes periodically depending on the position of the particle in its orbit. In our scenario, v is approximately 5–10% of v_H but it can become as large as 30% for highly eccentric orbits once close to perihelion. This has a significant effect on the semimajor axis of the particle orbit causing a fast inward migration. However, the analytical equations that describe the evolution of a body in the general Stark problem gives a very accurate description of the evolution of eccentricity, pericenter longitude, inclination and nodal longitude. The secular solution, obtained by Belyaev & Rafikov (2010) after averaging the Hamiltonian of the system (see their Section 3.2), is briefly summarized hereinafter since it will help in interpreting the numerical results. The authors start their analytical development by aligning the constant force along the z -axis and find that the system admits 3 integrals of motion

$$K_z = \sqrt{(1 - e^2)} |\cos i| \quad (3)$$

$$I_H = (1 - K^2)(1 - K_z^2/K^2)\sin^2\omega \quad (4)$$

and the semimajor axis, where $K(t) = \sqrt{(1 - e(t)^2)}$ is the dimensionless total angular momentum which is not conserved, while K_z is conserved since the force is parallel to the z -axis. By solving the Hamilton equations, they find that K oscillates between a maximum and minimum value given by

$$K_{M,m}^2 = \frac{1 + K_z^2 - I_H^2}{2} \pm \left[\left(\frac{1 + K_z^2 - I_H^2}{2} \right)^2 - K_z^2 \right]^{1/2} \quad (5)$$

The maximum and minimum values of the angular momentum translates into minimum and maximum values of eccentricity which depend on the inclination of the ISM flux respect to the initial orbit. The time dependence of K is periodic and given by

$$K(t) = \frac{K_m^2 + K_M^2}{2} + \frac{K_M^2 - K_m^2}{2} \sin\left(4\pi \frac{t - t_0}{T_{stark}}\right) \quad (6)$$

The period of the cycle T_{stark} is

$$T_{stark} = \frac{4\pi m_g}{3S} \sqrt{\frac{GM_\odot}{a}} \quad (7)$$

where a is the orbital semimajor axis, G the gravitational constant, M_\odot the star mass and S is the constant force applied in the z -axis direction. T_{stark} is constant in the general Stark problem, but it will change with time when we deal with dust particles under the action of radiation and ISM forces because of the inward drift that reduces the semimajor axis a and tends to circularize orbits. As a reference, the average value of T_{stark} for the initial sample of 1 μm particles in our model is about 2.3 Myr. This means that the dust grains will achieve an eccentricity of about 1 on a timescale shorter than $T_{stark}/2 \sim 1.1\text{Myr}$. When their eccentricity is close to 1 they drift quickly inside.

Once derived K as a function of t , we can easily compute $e(t)$, $\omega(t)$ (from the constant I_H) and $i(t)$ (from H_z). The solution is closed by the equation that gives the node longitude as a function of $K(t)$

$$\Omega(K) = \arctan\left(\sqrt{\frac{(K^2 - K_m^2)(K_M^2 - K_z^2)}{K_M^2 - K^2)(K_m^2 - K_z^2}}\right) \quad (8)$$

Thanks to the secular integrability of the Stark problem we can interpret the evolution shown in Fig.2 and the density plots in Fig.1. In the planar case, the maximum value of eccentricity $e_M = 1$ and the dust particles follow the evolution predicted by the equations of the Belyaev & Rafikov (2010) model in the (e, ω) plane. However, to properly compare the analytical solution of the Stark problem with our numerical results, we have to take into account the difference in the definition of inclination. The rule we adopt in this paper is that the inclination is counted from the orbital plane by a counter-clockwise rotation around the x -axis. As a consequence, $i = 0^\circ$ corresponds to $i = 90^\circ$ in the Belyaev & Rafikov (2010) model. This introduces a 180° difference in the definition of the perihelion longitude between our numerical solutions and the analytical formalism of Belyaev & Rafikov (2010). In Fig.2 the analytical curves for 3 different initial conditions in e and ω are shown as continuous lines with arrows pointing in the direction of the time flow. The particles move from an eccentricity of about 0.4 and, following the contours of constant H_z and I_H , evolve towards $e = 1$ while the pericenter tends towards the asymptotic value of 270° .

This behaviour explains why the shape of the disk in the density plots, for low values of τ , appears as a superposition of two ellipses. Most particles cluster either from below or from above around the fixed pericenter value of 270° . This alignment was also predicted by Scherer (2000) and observed in Maness et al. (2009). Thanks to the analytical solution of Belyaev & Rafikov (2010) it is possible to predict the angle between the two elliptical shapes that stand out in Fig.1. The analytical curves that enclose, for large eccentricities, all the particles, give for $e = 1$ a value of $\omega \sim 244.5^\circ$ and $\omega \sim 295.5^\circ$. Since most of the particles cluster close to these two curves, the angular separation between the two ellipses of Fig.1 is approximately 51° . A shortcut to obtain the angular separation is to use directly the formula (33) of Belyaev & Rafikov (2010) that, in the planar case, links eccentricity and perihelion to their constant initial values through the equation $e\cos\omega = \Lambda$ where Λ is the value of $e\cos\omega$ at $t=0$. By checking Fig.2, we notice that the curves leading to the outer edges of the peak in the (e, ω) plane approximately evolve from the following points: $(0.43, 180^\circ)$ and $(0.43, 360^\circ)$. Using these as starting values to compute Λ , we get $\Lambda = \pm 0.43$. As a consequence, the asymptotic values of ω , when e approaches 1, are $\omega \sim \arccos(0.43) \sim 64.5^\circ + 180^\circ = 244.5^\circ$ and $\omega \sim \arccos(-0.43) \sim 295.5^\circ + 180^\circ = 295.5^\circ$. The same value of separation of $\sim 51^\circ$ is obtained.

When the eccentricity becomes large, particles begin to drift inwards towards the star at increasing speed because of the strong PR drag and ISM perturbations on the semimajor axis. There is a larger variation in the difference between the orbital and ISM velocity over an orbit, and this causes an increasingly faster inward drift of grains. This explains why

the size of the disk, for small optical depths, is smaller even if more asymmetric.

In our model, when the particles have a semimajor axis smaller than 20 AU they are removed from the representative sample and a new particle is drawn. This limit is related to the large eccentricity of these particles when they have drifted inside. With a semimajor axis of 20 AU and an eccentricity of 0.9 they are very close to the star. It is expected that in this situation the dust particles may either sublimate or be scattered by internal planets. According to Kobayashi et al (2009); Mukai (1996) micron-sized dust grains consisting of a silicate core with an icy mantle may undergo active sublimation at temperatures higher than 110 K. This temperature is estimated to be present on the surface of a $1 \mu\text{m}$ grain at about 20 AU from a solar type star. This scenario, however, does not easily apply to dust particles perturbed by ISM. They are on highly eccentric orbits while Kobayashi et al (2009) consider grains on circular orbits and perturbed by PR drag only. In our model, the drift timescale is very short since, in addition to PR drag, a strong contribution to the drag force is given by the ISM perturbations and we expect that the particles have a rapid infall towards the star when an eccentricity larger than 0.9 is achieved. It appears a complex issue to predict the amount of sublimation in this context and compare it to the drift timescale. For simplicity, we assume that when the semimajor axis of a dust particle crosses the lower limit of 20 AU a series of mechanisms would make its contribution to the outer disk negligible. A test run where this limit was lowered to 15 AU did not change the outcome in terms of density plots. Scattering by planets appear also a reasonable outcome when particles move close to the star. The presence of a debris disk is a strong indication that planetary formation occurred in the system. It is then expected that a planetary system orbits the star at some distance from it. The potential planets would intercept the dust particles as they get close to the star eliminating them from the disk population.

When we consider larger particles, a different balance between perturbative changes due to ISM and lifetime is reached. In addition, the initial disk is expected to be less radially spread since the value of β is smaller and the initial orbital elements of the grains are closer to those of the parent bodies. In Fig.3 we show density plots of a dusty disk made of $10 \mu\text{m}$ size particles ($\beta = 0.03$). If the optical depth is set to $\tau = 10^{-3}$ the disk does not show any difference from the case where ISM is neglected since the ISM perturbations do not have enough time to build up a consistent variation of eccentricity and perihelion. It appears as a regular ring almost overlapping with the parent body ring. The initial eccentricities are close to 0 because of the small value of β so that the disk appears circular and the overdense rings observed in Fig.1, top left plot, are not present. For a smaller optical depth, $\tau = 10^{-4}$, eccentricities as large as 0.15 are pumped up by the ISM perturbations and the disk appears slightly eccentric. When finally $\tau = 10^{-6}$, the orbits of the grains reach a maximum eccentricity of ~ 0.8 and a significant clump develops close to the apocenter of the orbits. In this case, the two-ellipse pattern, observed for $1 \mu\text{m}$ in Fig.1 bottom-right plot, collapses into a single elliptical structure. The explanation for this different behaviour resides in the lower initial eccentricity with which $10 \mu\text{m}$ are produced.

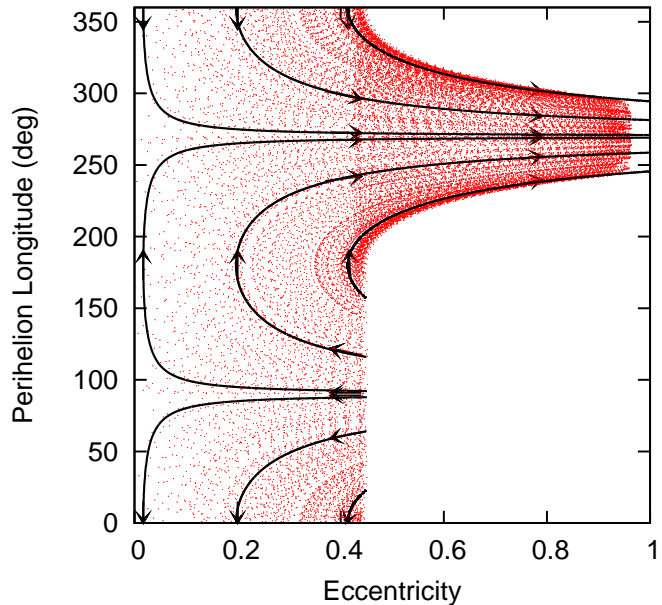


Figure 2. Evolution in the (e, ω) plane of 100 sampled dust particles. The orbital elements are computed over an interval of time of 5 Myr. The optical depth τ is set to 10^{-6} to grant enough time to the grains to dynamically evolve.

This is about 0.03, small compared to the average value of about 0.4 for $1 \mu\text{m}$ particles. By inspecting Fig.2 we notice that the analytical curve of the Stark problem for particles passing through low eccentricities gives values of perihelion very close to 270° when the eccentricity approaches 1. All grains in the $10 \mu\text{m}$ case evolve from low eccentricity values and when their eccentricity is pumped up by the ISM perturbations, their pericenter is almost perfectly aligned to 270° . Exploiting again formula (33) of Belyaev & Rafikov (2010), when $e = 0.03$, we get an angular separation between the 2 streams of particles, approaching $\omega = 270^\circ$ for large eccentricities, of only $\sim 4^\circ$. As a consequence, in the density plot the two ellipses merge in a single one.

The behaviour shown in Fig.3 confirms that the optical depth τ is the critical parameter in determining the amount of asymmetry produced by the ISM flux on a dust disk even for larger sizes of the dust particles. When τ is large, the effects of the ISM flux become negligible and the debris disk appears symmetric.

5 THE INCLINED CASE

When the ISM flow is inclined of an angle i_{ISM} respect to the parent body plane, the analytical model of the Stark problem predicts an increase of the grain orbital inclination and a reduction of the maximum value of the eccentricity (Belyaev & Rafikov 2010). The 2-D model, described in the previous section, continues to be a good approximation only when i_{ISM} is lower than 10° . For larger values, the ISM perturbations lead to 3-dimensional effects that alters the density distribution patterns observed in Fig.1 and, in addition, cause significant warping of the disk. However, if the optical depth τ is of the order of 10^{-3} , the collisional disruption prevents the building up of significant inclination,

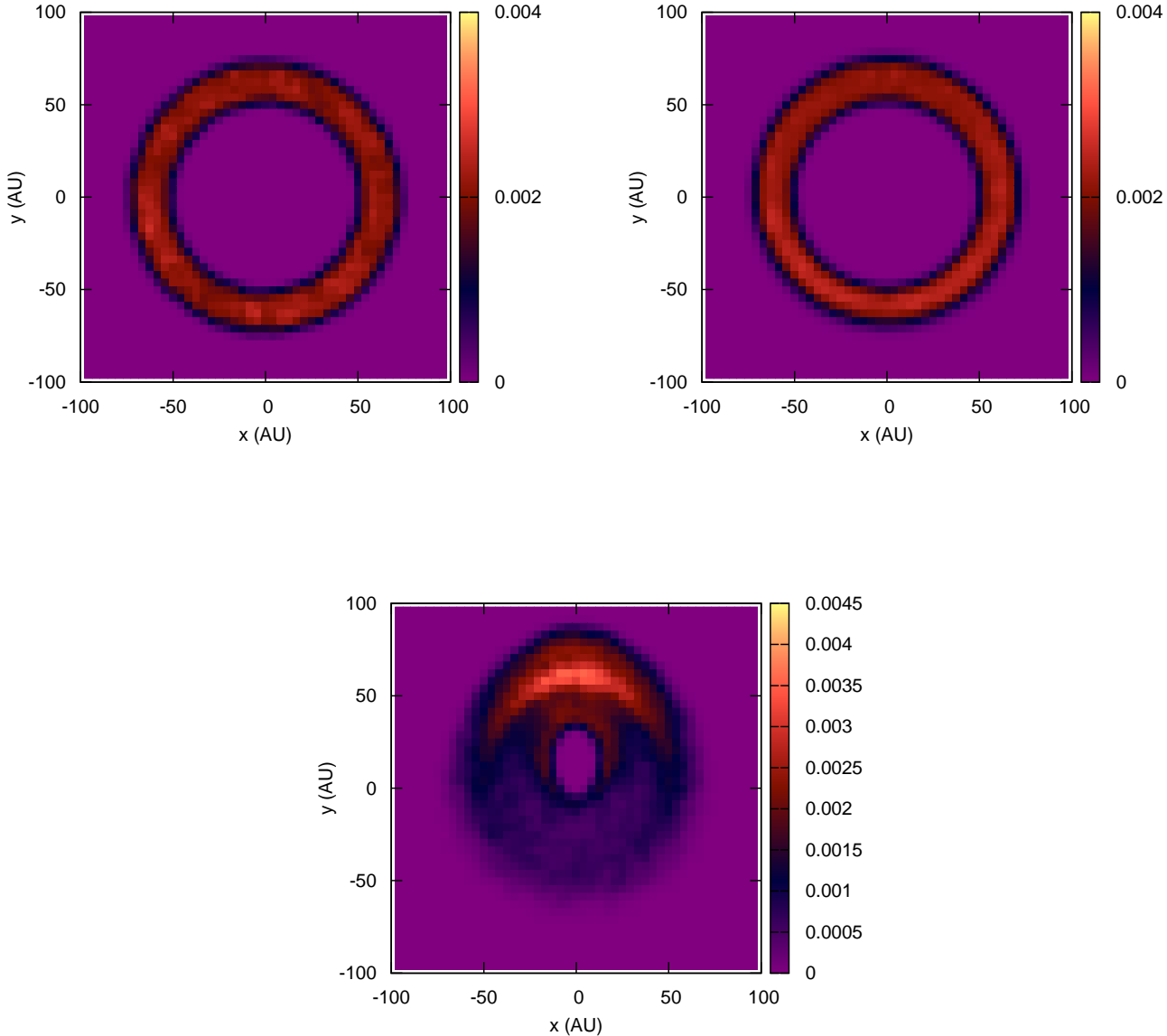


Figure 3. 2-D density distribution of $10 \mu\text{m}$ size dust particles when a steady state is reached. The top-left plot shows the case with optical depth $\tau = 10^{-3}$, the top-right plot that with $\tau = 10^{-4}$. The last and more perturbed case shown in the bottom plot corresponds to an optical depth of $\tau = 10^{-6}$. This figure has to be compared with Fig.1.

as it does for the eccentricity, and the warping of the disk is negligible.

This is shown in Fig.4 where the outcome of a simulation with $i_{ISM} = 60^\circ$ and $\tau = 10^{-3}$ is illustrated as a density plot in the $(x - z)$ plane. Only small out-of-plane features can be detected in the figure which cannot be interpreted neither as warping or clumping due to their limited extension along the z -axis (the scale along the z -axis is $1/10$ of the scale along the x -axis). A large optical depth prevents then a disk to develop structures not only in the parent plane but also out-of-plane. This finding is confirmed

for any value of i_{ISM} . In Fig.5 the median inclination of the grains in the disk is plotted for different values of i_{ISM} with $\tau = 10^{-3}$ (top plot). The value of the median of the particle inclinations is always smaller than 5° since the Stark cycle is quickly interrupted by a collision. This confirms that if the disk is optically thick, the ISM does not have time to build up observable signatures in the density distribution of debris disks. In addition, the particles do not have the time to drift inside since they are destroyed before PR drag and the ISM drag force them to migrate inside. If a gap is present

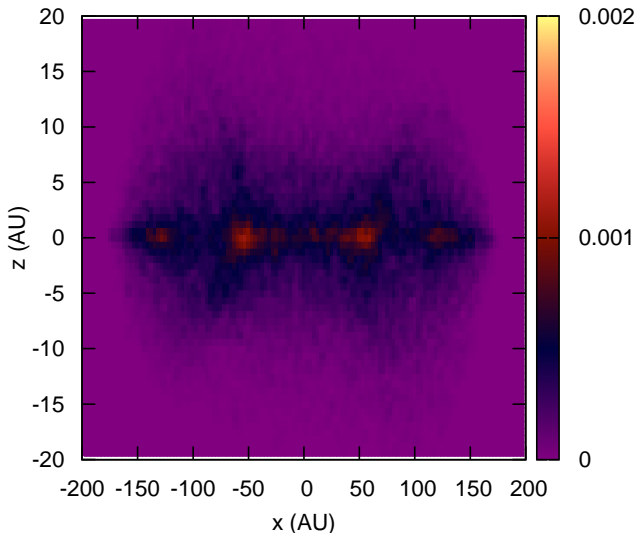


Figure 4. Density distribution in the $(x-z)$ plane when $\tau = 10^{-3}$. The quick collisional disruption prevents large out-of-plane structures to develop. Notice that the scale along the z -axis is 1/10 of the scale along the x -axis.

in the inside regions of the disk this will not be filled up by the grain migration.

Significantly different is the situation when τ is as low as 10^{-6} (Fig.5 bottom plot): particles in the disk have time to move along the Stark cycle. This is not interrupted by collisions since the collisional lifetime is longer than T_{stark} and the particles can build up large orbital eccentricities and inclinations. In this scenario, the only mechanism able to halt the Stark cycling is the fast inward drift due to the large eccentricity. The particles migrate inside driven by the PR and ISM drag forces ending either onto the star or sublimating or impacting onto a planet. This sink mechanism is more effective for smaller values of i_{ISM} since the maximum eccentricity e_{max} that can be achieved by the particles decreases for increasing i_{ISM} , according to the Stark general problem. In Fig.6 we show the evolution of the eccentricity and inclination for increasing values of i_{ISM} . Their values are strongly correlated, as predicted by the theory of Belyaev & Rafikov (2010) (the theoretical curves are plotted as continuous lines in the figures).

Two interesting features come out from Fig.6. First of all the drag forces tend to reduce the eccentricity detaching the numerical data from the theoretical curve even if the difference is not very marked. In addition, when the maximum eccentricity is lower, for higher i_{ISM} , the particles move farther within the Stark cycle because their drift time is longer. When $i_{ISM} = 90^\circ$ the particles complete a full cycle and some start a new one, even if they do not complete more than two cycles before drifting inside 20 AU.

Additional features related to the dynamics of the dust particles under the action of the ISM flow and PR drag can be seen in the density plots shown in Fig.7. In the parent

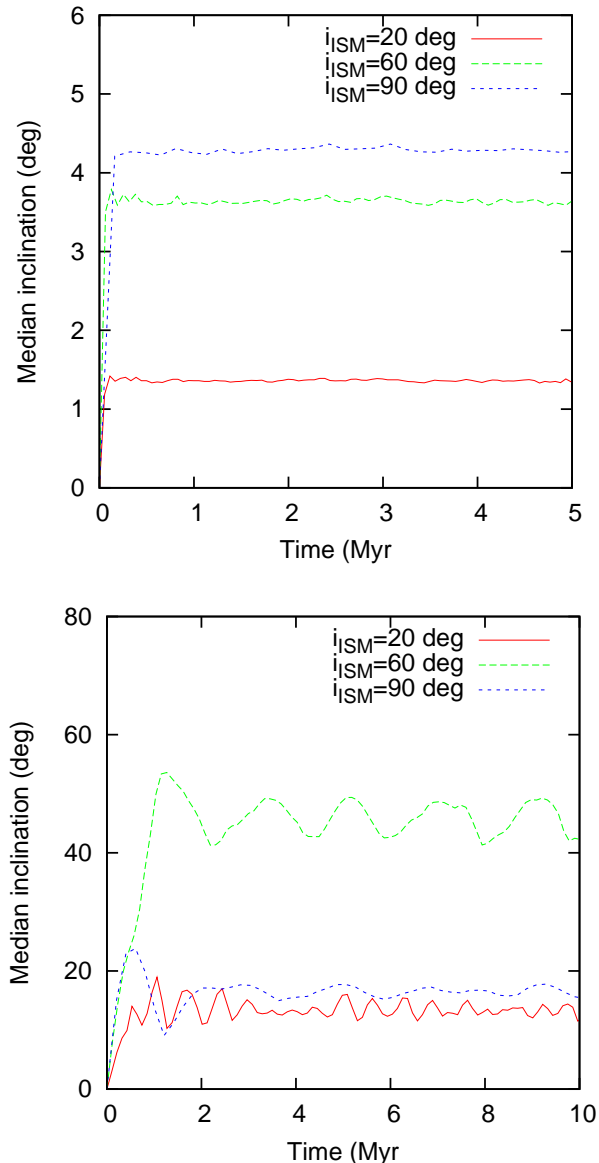


Figure 5. Median inclination in a dust disk of 1 μm size particles for different values of i_{ISM} and τ . In the top plot $\tau = 10^{-3}$ while in the bottom one it is $\tau = 10^{-6}$.

body plane the density distribution appears very asymmetric. In the case where $i_{ISM} = 20^\circ$ (Fig.7 top plots) it is still possible to recognize the two elliptical structures produced by the evolution in the (e, ω) plane but their shape is blurred due to the inclination distribution. However, when $i_{ISM} = 60^\circ$ the double-elliptical structure has fully disappeared and the inclination distribution determines the density distribution also in the parent body plane. As it can be argued from Fig.6 middle plots, the orbital inclination is concentrated around $i \sim 50^\circ$ and, in addition, when the inclination is higher, the node longitude is clustered around $\Omega = \pi/2$. This leads to an eccentric disk structure that is inclined respect to the original orbital plane of the parent body of approximately 50° . Finally, the case $i_{ISM} = 90^\circ$ (Fig.6 bottom plots) is the most symmetric case. The circular overdense shape of the disk close to the star is where

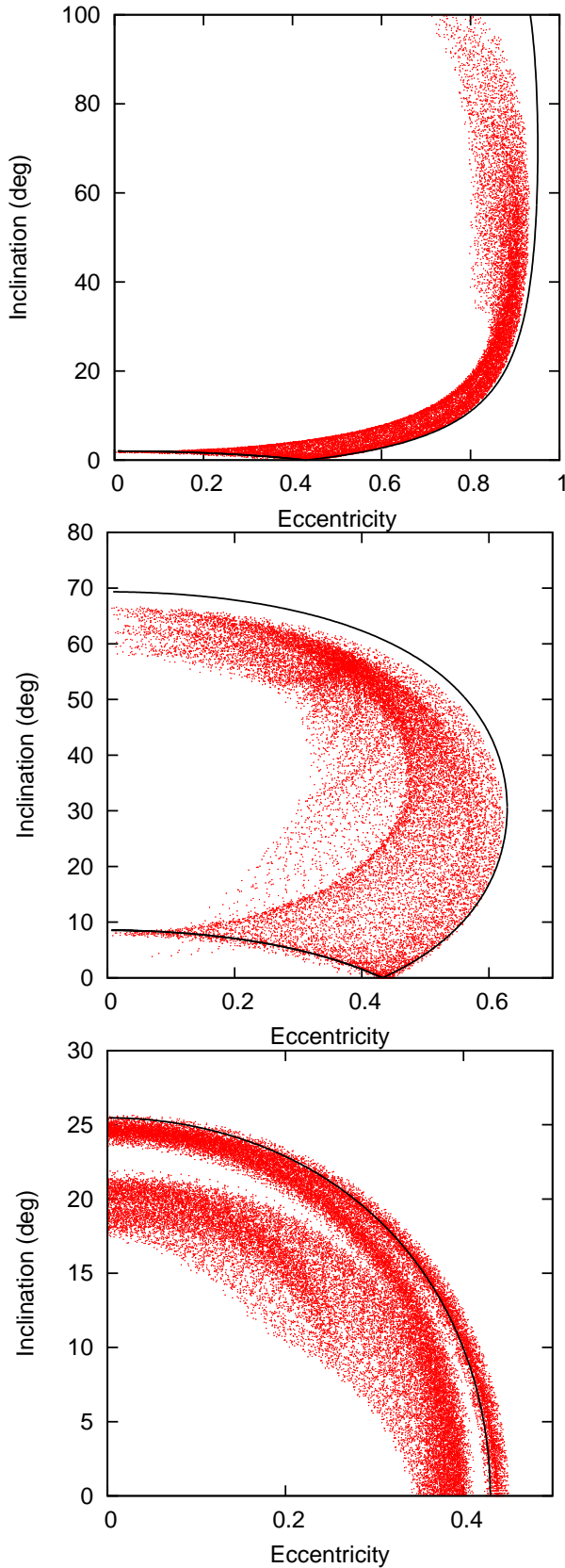


Figure 6. Correlation between the eccentricity and inclination for dust particles in a disk with different values of i_{ISM} . In the top plot $i_{ISM} = 20^\circ$, in the middle $i_{ISM} = 60^\circ$ and in the bottom $i_{ISM} = 90^\circ$. The continuous lines are the theoretical predictions derived from the analytical theory of the Stark problem.

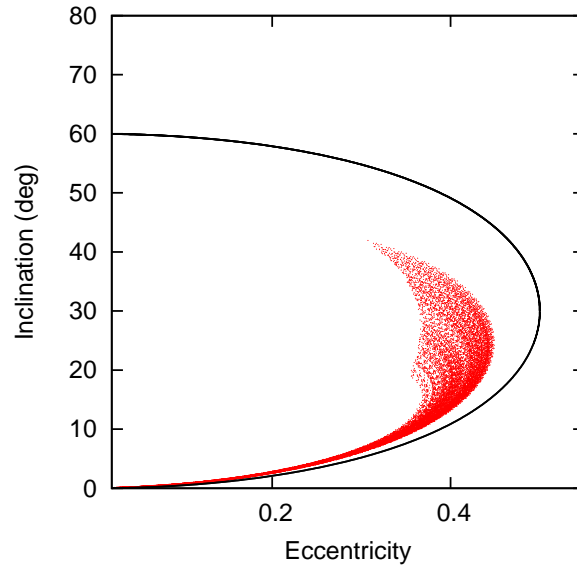


Figure 8. Eccentricity–inclination distribution for $10 \mu\text{m}$ size dust particles in a disk with $i_{ISM} = 60^\circ$.

the inclined orbits cross the parent body plane. The dust particles have a statistical uniform distribution of the nodes for any value of inclination and, as a consequence, a high density region is formed in correspondence to the intersection between the inclined orbits and the initial parent body plane.

For larger dust grains ($10\mu\text{m}$) and low optical depth ($\tau = 10^{-6}$), the dynamical scenario is slightly different. The Stark period is of the order of 23 Myr, 10 times longer than that of $1\mu\text{m}$ particles, but the drift rate has not decreased by the same amount. As a consequence, the grains evolve less into the Stark cycle and migrate inside before reaching large values of inclination. This is shown in Fig.8 where the eccentricity and inclination of the dust, when the disk is in a steady state, are illustrated. The initial eccentricity is close to 0 since β is small and this leads to a different Stark cycle compared to that in Fig.6 middle plots. The particles slowly evolve towards larger inclination values but they plunge into the inner regions of the disk and are lost before they can develop significant inclinations. The disk is then expected to be less perturbed compared to the case for $1 \mu\text{m}$ size particles. This is confirmed by Fig.9 where the spatial density distribution is illustrated and can be compared to that shown in Fig.7 (middle plot) for $1 \mu\text{m}$ size particles.

6 CONCLUSIONS

We have shown in this paper, by numerical modeling the evolution of debris disks under the effects of solar radiation pressure, PR drag and ISM flux, that for typical values of optical depth $\tau \sim 10^{-3}$ the signatures of the ISM wind on grains with radius in the range $1 - 10 \mu\text{m}$, just above the cut-off size imposed by radiation pressure, are almost negligible. The amount of perturbations due to the interaction of dust particles with the local ISM neutral atom flow are strongly reduced when the grain lifetime is short as in disks with large

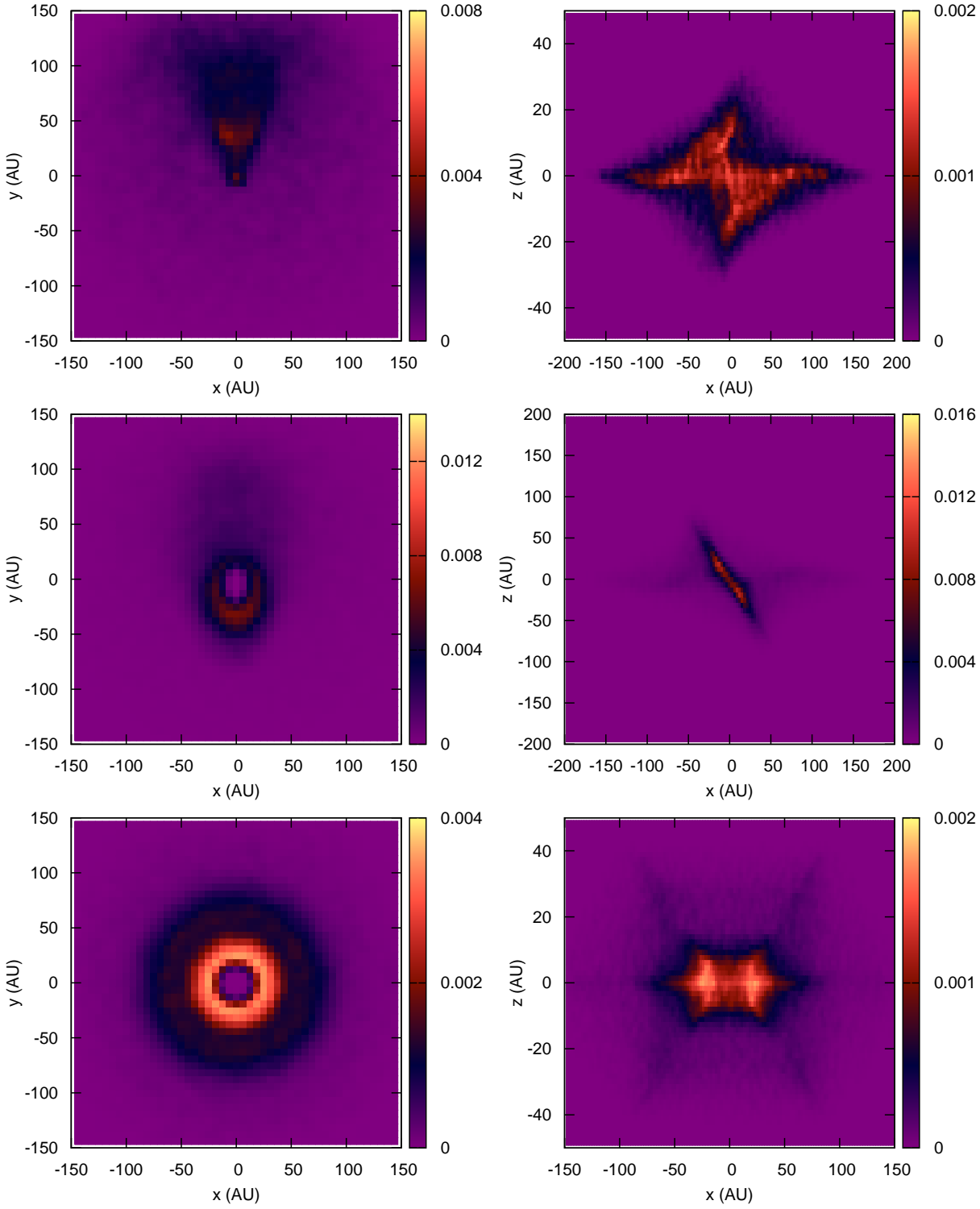


Figure 7. Density distributions of $1 \mu\text{m}$ size dust particles in the $(x-y)$ and $(x-z)$ plane for different values of i_{ISM} . The top plots refer to the case $i_{ISM} = 20^\circ$, the middle plots to $i_{ISM} = 60^\circ$ and the lower plots to $i_{ISM} = 90^\circ$, respectively.

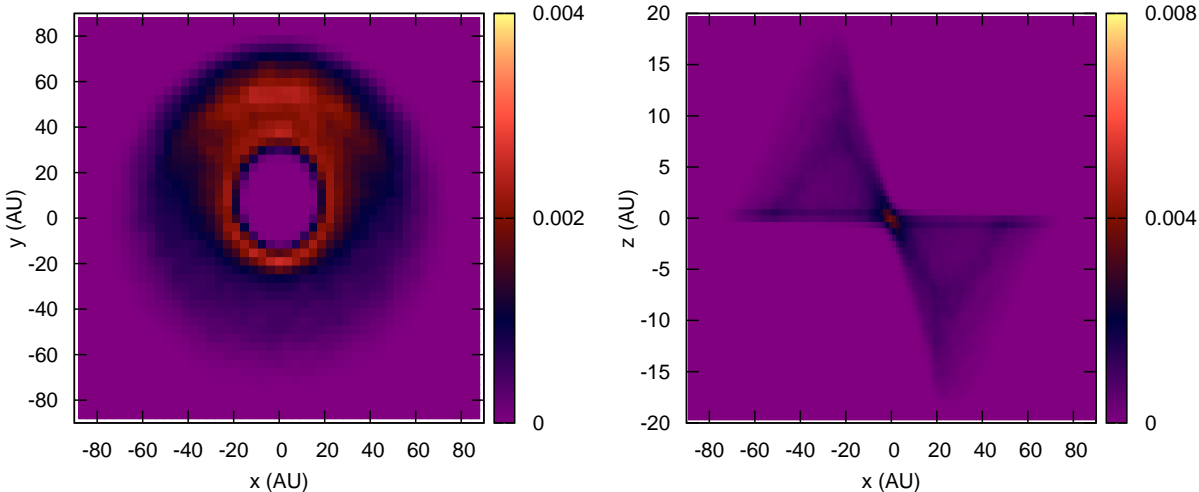


Figure 9. Density distributions of $10 \mu\text{m}$ size dust particles in the $(x-y)$ and $(x-z)$ plane for $i_{ISM} = 60^\circ$. These distributions can be compared to those for $1 \mu\text{m}$ shown in Fig.6 middle plots.

values of τ . In this scenario, the presence of asymmetries must be ascribed to different mechanisms like the presence of massive bodies within the disk. The neutral ISM fails in producing either warping or clumping in such disks.

Different is the scenario when the optical depth is small. We have shown that for $\tau \sim 10^{-6}$ significant asymmetries appear on the density profile of the disk both in the parent bodies plane and out-of-plane. Interesting is a double-elliptical pattern that develops in the parent bodies plane when the ISM flow is almost coplanar to it. The disk structures are caused by the dynamical evolution of the orbital elements of the dust grains. The way in which these orbital parameters evolve can be in part predicted on the basis of the general Stark model that helps in understanding the periodic nature of eccentricity, inclination and the dynamically related angles perihelion argument and nodal longitude (Belyaev & Rafikov 2010; Pastor 2011). In addition, the semimajor axis has a fast inward drift due to the combination of PR drag and interaction with the ISM. The two drag forces, in particular that related to the ISM flow, are strong because of the large eccentricity of the grains. The particles quickly migrate towards the star where they can either sublimate or be destroyed by collisions with planets or the star itself. This is an additional powerful sink mechanism for debris disks with small optical depth. On the contrary, if the disk has a large optical depth, collisional disruption acts on a much shorter timescale and it prevents a significant inward migration. The disk shape in this case would be mostly due to the initial value of β which sets the initial orbital element distribution of the grains. The debris disk would then extend outwards respect to the parent body ring in spite of the strong ISM and radiation drag force. This additional different dynamical behaviour of the dust grains, which again depends on the optical depth, sets a nice correlation between the value of τ and location of the disk respect to the parent

body ring. Disks with low values of τ would expand inward respect to the parent body ring down to the sublimation region or where planets are orbiting, while disks with large values of τ would extend mostly outwards.

Our study suggests that observational data of debris disks need care to be interpreted. Potential asymmetries identified in the density distribution may be ascribed to interactions with the local flux of ISM neutral atoms surrounding its parent star only if the disk has a low optical depth. Otherwise, alternative explanations, like the presence of planets, must be investigated.

ACKNOWLEDGMENTS

We thank Mikhail Belyaev for his useful comments and suggestions while acting as referee of the paper.

REFERENCES

- Artymowicz P. and Clampin M., 1997, ApJ 490, 863.
- Belyaev, M.A. and Rafikov R.R., 2010, ApJ 723, 1718
- Debes J.H., Weinberger A.J., and Kuchner M.J., 2009, ApJ. 702, 318.
- Draine B.T. and Salpeter E.E., 1979, ApJ. 231, 77.
- Everhart E., 1985. In: Carusi A., Valsecchi G.B. (eds.) Proc. IAU Coll. 83, Dynamics of comets: their origin and evolution. Reidel, Dordrecht, p.185
- Fhar H.J., 1996, Space Sci. Rev. 78, 199
- Frisch P.C., Dorschner J.M., Geiss J., Greenberg J.M., Grun E., Landgraf M., Hoppe P., Jones A.P., Kratschmer W., Linde T.J., Morfill G.E., Reach W., Slavin J.D., Svestka J., Witt A.N., Zank G.P., 1999, ApJ 525, 492.
- Kobayashi H., Watanabe S., Kimura H., Yamamoto T., 2009, Icarus 201, 395.

- Lallement R., Quemerais E., Bertaux J.L., Ferron S., Koutroumpa D., Pellinen R., 2005, *Science* 307, 1447
- Maness H.L., Kalas P., Peek K.M.G., Chiang E.I., Scherer K., Fitzgerald M.P., Graham J.R., Hines D.C., Schneider G., Metchev S.A., 2009, *ApJ* 707, 1098.
- Marzari F. and Vanzani V., 1994, *A&A* 283, 275.
- Mukai T., 1996, *Physics, Chemistry and Dynamics of Interplanetary Dust*, ASP Conference series, 104 (Gustafson and Hanner Eds.), 453.
- Pastor, P., 2011, arXiv:1012.1246v1,
- Scherer K., 2000, *JGR* 105, 10329.
- Thebault P. and Augereau J.-C., 2007, *A&A* 472, 169.
- Wyatt M.C., 2005, *A&A* 433, 1007
- Wyatt M.C., 2008, *ARAA* 46, 339